Physica B 415 (2013) 38–43

Contents lists available at SciVerse ScienceDirect

Physica B

journal homepage: www.elsevier.com/locate/physb

Isothermal annealing of a 620 nm optical absorption band in Brazilian topaz crystals

Sadao Isotani [a,*], Masao Matsuoka [a], Antonio Roberto Pereira Leite Albuquerque [b]

[a] Instituto de Física, Universidade de São Paulo, São Paulo, Brazil
[b] University Federal of São Paulo, São Paulo, Brazil

ARTICLE INFO

Article history:
Received 7 June 2012
Received in revised form
23 November 2012
Accepted 18 January 2013
Available online 9 February 2013

Keywords:
Topaz
Polaron
First order kinetics
Optical absorption
Thermoluminescence

ABSTRACT

Isothermal decay behaviors, observed at 515, 523, 562, and 693 K, for an optical absorption band at 620 nm in gamma-irradiated Brazilian blue topaz were analyzed using a kinetic model consisting of O^- bound small polarons adjacent to recombination centers (electron traps). The kinetic equations obtained on the basis of this model were solved using the method of Runge–Kutta and the fit parameters describing these defects were determined with a grid optimization method. Two activation energies of 0.52 ± 0.08 and 0.88 ± 0.13 eV, corresponding to two different structural configurations of the O^- polarons, explained well the isothermal decay curves using first-order kinetics expected from the kinetic model. On the other hand, thermoluminescence (TL) emission spectra measured at various temperatures showed a single band at 400 nm in the temperature range of 373–553 K in which the 620 nm optical absorption band decreased in intensity. Monochromatic TL glow curve data at 400 nm extracted from the TL emission spectra observed were found to be explained reasonably by using the knowledge obtained from the isothermal decay analysis. This suggests that two different structural configurations of O^- polarons are responsible for the 620 nm optical absorption band and that the thermal annealing of the polarons causes the 400 nm TL emission band.

1. Introduction

Topaz is a silicate class mineral with the following chemical formula, $Al_2(F, OH)_2SiO_4$ [1]. The coloration phenomena in this mineral caused by defects induced by ionizing irradiation have been the subject of extensive studies. The first study remounts to early 1923 [2], describing coloration from brown smoke to orange shades in topaz. In 1975, Nassau and Prescott reported a remarkable feature obtained from 86 colorless topaz samples with the probable origin of Brazil; 21 samples exhibited blue colorations after gamma irradiation followed by moderate heating (blue topaz) [3].

The detailed investigation of atomic models for point defects in topaz began only in 1990 when Priest et al. attributed the defect responsible for the 620 nm absorption band to an oxygen vacancy in an isolated SiO_4 tetrahedron, in the form of a doubly occupied dangling silicon bond [4]. Later, from some studies of the irradiation effects in natural colorless and blue topaz from different locations in Brazil using electron paramagnetic resonance (EPR) and optical absorption, Krambrock et al. showed that the 620 nm absorption band induced by neutron or gamma irradiation is responsible for the blue color in topaz; a paramagnetic O^- hole center is formed at a hydroxyl OH^- lattice site removing the hydrogen atom from the OH^- ion; the O^- hole center has the same thermal stability as the 620 nm absorption band [5–7].

Further, Schirmer developed a model of O^- hole centers in oxide materials, that is, a hole is trapped in a cluster of a few equivalent oxygen ions next to an acceptor defect and is stabilized by lattice distortion as an O^- bound small polaron [8]. Accordingly, Krambrock et al. discussed the 620 nm absorption band and O^- hole centers in the context of O^- bound small polarons and reported that: neutron irradiation causes some intrinsic damage or precursor defects such as vacancies responsible for the stability of the O^- hole centers; gamma irradiation produces O^- hole centers near natural damage or electron trapping sites and this depends strongly on the origin of topaz [9].

It is well known that: heating of natural colorless topaz between 470 and 573 K and subsequent gamma irradiation does not affect the 620 nm absorption band, while heating above 573 K before irradiation leads to reduction of this band in intensity [10]. This may suggest that the lattice distortion stabilizing the O^- hole center might be reduced at temperatures above 573 K, resulting in the reduction in intensity of the 620 nm optical absorption band.

In this work we have analyzed the isothermal decay curves, obtained at 515, 523, 562, and 693 K, for the 620 nm absorption band in blue topaz, using a kinetic model involving O^- hole centers and recombination centers (electron traps). This model is

* Corresponding author. Fax: +55 11 3813 4334.
E-mail addresses: sisotani@if.usp.br, sisotaniifuspbr@gmail.com (S. Isotani).

0921-4526/$ - see front matter © 2013 Elsevier B.V. All rights reserved.
http://dx.doi.org/10.1016/j.physb.2013.01.040

similar to that proposed by Adirovitch [11] and leads to two coupled differential equations with the parameters characterizing these defects; these equations are known to have the exact numerical solutions [12]. Moreover, thermoluminescence (TL) emission spectra measured have been found to exhibit a single band at 400 nm in the range of 373–553 K in which the 620 nm absorption band decreases in intensity. Accordingly, we have simulated monochromatic TL glow curve data at 400 nm extracted from the TL emission spectra, using the knowledge obtained from the isothermal decay analysis, to demonstrate the correlation between the 400 nm TL emission and 620 nm absorption bands.

2. Experimental

All the topaz materials, showing colorless or slightly brown, were obtained in the region around Governador Valadares, Minas Gerais, Brazil. The results of impurity analyses for the materials are reported in a previous work [13], indicating the presence of the impurities Fe (200–380 ppm), Cr (100 ppm) and Mn (60 ppm).

Specimens of 1–5 mm in thickness used in this study were cut from the materials using a diamond saw and polished using chromium oxide, alumina and diamond pastes. All the specimens thus prepared were previously irradiated at room temperature to some 10^7 Gy using a ^{60}Co gamma source (1.48×10^{16} Bq) at a dose rate of 8.0×10^4 Gy/h. The absorbed dose was determined with ceric-cerous, AECL red acrylic, and UKAEA red perspex dosimeters. Heat treatments for the specimens previously irradiated were made with an electric furnace in air at a temperature 373–473 K during 24 h in order to obtain the crystal blue color in the specimens.

The isothermal treatments of blue topaz samples were accomplished at 515, 523, 562, and 693 K in the way described below. In first place we checked thermal stability (within ±1 K) of an electric furnace with an internal volume of $0.10\times0.12\times0.15$ m^3 in which two plates of iron were maintained. Each sample was treated at each constant temperature, being sandwiched in the plates of iron. It is confirmed in this case that the rise time from room temperature to the highest treatment temperature was about 20 s; the sample temperature was measured using a thermocouple type K with reference to a mixture of water and ice. When a desired treatment time was accomplished, the sample was immediately taken out from the electric furnace, put between other two plates of iron at room temperature, and cooled down to room temperature. After each step of the successive isothermal treatments of the sample, the optical absorption spectrum of the sample was measured at room temperature with a Varian Cary 17D spectrometer. The isothermal decay curve, that is, the 620 nm optical absorption band intensity as a function of the accumulated time of successive isothermal treatments at a certain temperature, could be obtained in this manner.

On the other hand, a heating device with an electrical resistance for the sample was introduced into the sample chamber of the Varian Cary 17D spectrometer to perform measurements of the TL emission spectra at various temperatures during the heating. The sample temperature was monitored using a thermocouple type K. Due to operational reasons it was not always possible to maintain the heating rate constant, as shown in Fig. 1. The temperature variation during each TL emission spectrum measurement was about 3%. In Section 5 monochromatic TL glow curve data at 400 nm, extracted from the TL emission spectra measured, will be simulated with model of the isothermal decay analysis results and the detail of the simulation procedure using this heating manner depicted in Fig. 1 will be shown.

3. Results

3.1. Optical absorption

Fig. 2 shows a typical optical absorption spectrum for a blue topaz sample. In the figure the well-defined absorption band is observed at 620 nm under the influence of a strong absorption in the ultraviolet region. A recent study indicates that the strong absorption observed below 400 nm in the present spectrum is due to an optical absorption band around 314 nm and that this band can be tentatively assigned to silanone (=Si=O) [14]. A small and broad shoulder of the 620 nm band appears in the region of 800–1100 nm. In this region some peaks of Fe^{2+} in octahedral sites are observed in several minerals [15–18] and hence we suggest that this shoulder should be attributed to this Fe^{2+}. Further, a sharp band at 1209 nm (8271 cm^{-1}) and a small band at 1226 nm (8157 cm^{-1}) are assigned to a combination band of the first overtone of the stretching mode of OH^- (3644 cm^{-1}) [19] and the bending mode of Al−OH (1160 cm^{-1})

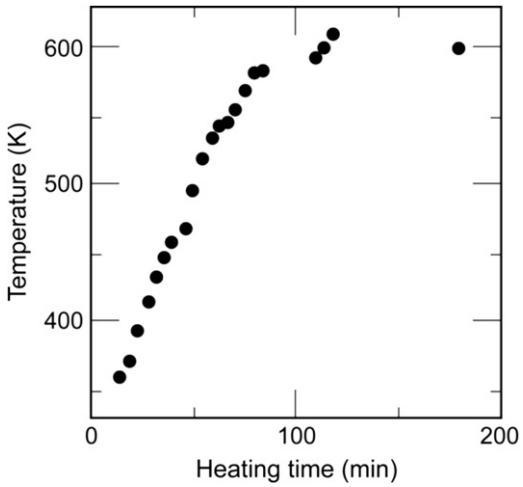

Fig. 1. Heating curve used for the measurement of TL emission spectra.

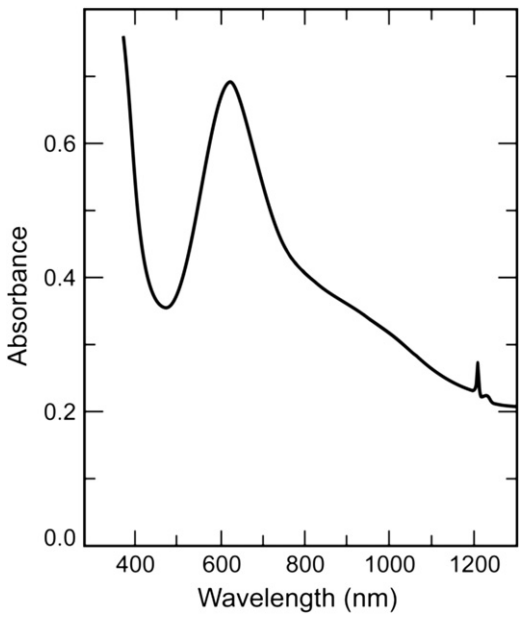

Fig. 2. Typical optical absorption spectrum, with a well-defined 620 nm band, for a blue topaz sample.

[20], and that of the first overtone of the stretching mode of OH^- and a very weak band observed at 1079 cm^{-1} in some topaz samples [20], which is attributed to the bending mode of Al–OH, respectively. The details will be described in a forthcoming article.

3.2. TL emission spectra

TL emission spectra observed for a blue topaz sample are shown in Fig. 3. It is interesting to note from the figure that: (1) a TL emission band at 400 nm is singly observed in the temperature range of 373–553 K [Fig. 3b], in which the 620 nm absorption band decreases in intensity; (2) another TL emission band at 800 nm starts appearing above 553 K [Fig. 3c and d]. As mentioned above, heating of natural topaz above 553 K before irradiation inhibits the formation of the 620 nm absorption band, and hence the 800 nm TL emission band may be related to the thermal destruction process of precursors for the 620 nm absorption band. However, further investigation of the 800 nm TL emission band is necessary.

3.3. Isothermal decay of 620 nm optical absorption band

The isothermal decay results obtained at 515, 523, 562, and 693 K for the 620 nm absorption band are shown in Fig. 4. In the figure, the absorption band intensity is normalized to that registered before any isothermal treatment and the solid lines are the simulation results obtained from the analysis through the kinetic model which will be described in the following section.

4. Analysis of isothermal decay of 620 nm optical absorption band

As mentioned in Section 1, the 620 nm absorption band in blue topaz is attributed to the O^- hole centers which can be produced by neutron or gamma irradiation and stabilized by defects [9]. To explain the isothermal decay results obtained, we consider that

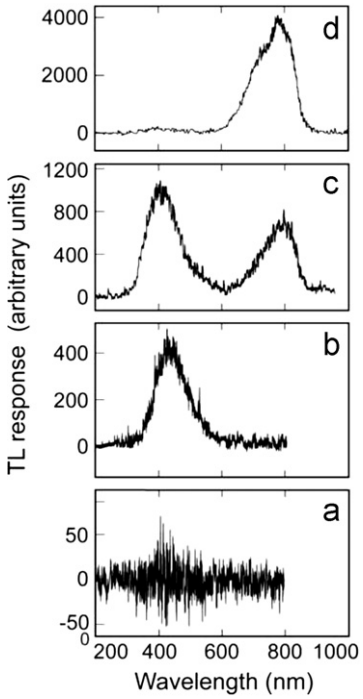

Fig. 3. TL emission spectra for a blue topaz sample. The time and temperature at the beginning of each recording are (a) 42 min and 443 K, (b) 49 min and 468 K, (c) 89 min and 598 K, and (d) 119 min and 632 K.

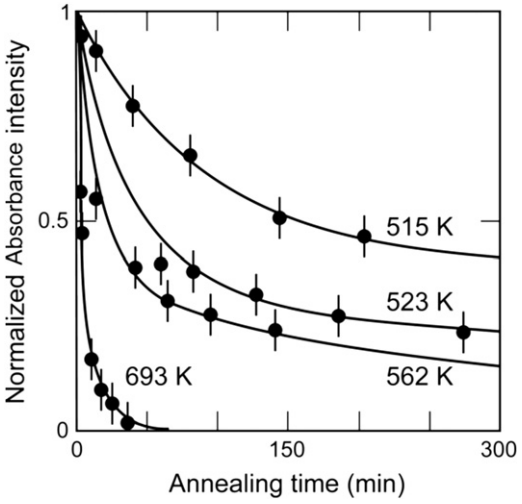

Fig. 4. Normalized isothermal decay curves for 620 nm absorption band, observed at 515, 523, 562, and 693 K, as a function of the accumulated time of the heat treatment (dots). Each solid line indicates the simulation result.

holes are thermally released from the O^- hole centers (filled hole traps) and move through the valence band until being retrapped into O^{2-} traps (unfilled hole traps) or being recombined with electrons in the recombination centers (electron traps). This recombination process causes the photon emission (TL) which we may expect to be the 400 nm TL emission band. This scheme is similar to that used for the analysis of the reduction process from Fe^{3+} to Fe^{2+} ions in beryl [21]. The O^- hole centers in topaz have several stabilized configurations and hence we consider N different structural configurations of the O^- hole centers and a single kind of recombination centers.

Using this model, the isothermal decay curves can be analyzed by solving a set of coupled differential equations through the numerical method of Runge–Kutta. This method has been applied with success to the analyses of thermal relaxation of: radiation-induced green color in spodumene [22], luminescence in spodumene [23], atomic hydrogen in glass and beryl [24], and F-center in LiF irradiated at room temperature [25,26].

Let us suppose that all the charges are in electrical equilibrium so that the concentrations of holes and electrons satisfy the relation:

$$y_e = \sum_{i=1}^{N} y_i + y_f, \tag{1}$$

where y_e is the concentration of electrons in the recombination centers, y_i is the concentration of holes trapped in the i-th configuration of hole traps and y_f is the concentration of free holes in the valence band.

The thermal release rate of holes from the filled hole traps in the i-th configuration to the valence band is given by $\alpha_i y_i$, where α_i is given by $\alpha_i = s_i \exp(-E_i/kT)$, where s_i and E_i are the frequency factor and activation energy of hole traps in the i-th configuration, respectively; k is the Boltzmann constant and T is the absolute temperature. The retrapping rate of the valence band holes is given by $\beta_i y_f (y_{0,i} - y_i)$, where β_i is the retrapping probability coefficient and $y_{0,i}$ is the total concentration of hole traps in the i-th configuration, and the recombination rate of free holes with trapped electrons is given by $\gamma y_f y_e$, where γ is the recombination probability coefficient.

The resulting rate equations are given by:

$$\frac{dy_i}{dt} = -\alpha_i y_i + \beta_i y_f (y_{0,i} - y_i), \text{ where } i = 1,2,\ldots,N, \tag{2a}$$

$$\frac{dy_f}{dt} = \sum_{i=1}^{N}[\alpha_i y_i - \beta_i y_f(y_{0,i}-y_i)] - \gamma y_f\left(\sum_{i=1}^{N} y_i + y_f\right). \quad (2b)$$

From the non-linear stability analysis applied to similar cases, these equations are known to have stable solutions [27]. The solutions of these equations follow hyperbolic paths, resulting in difficulty to find the solutions for large values of time and concentrations. Consequently, the rate equations should be normalized to time and concentrations. The initial conditions are $y_i=1\equiv y_{0,i}$ and $y_f=0\equiv y_{0,f}$ at time $t=0$ (*i.e.*, all the hole traps are filled and there is not any valence band hole) and the normalization factor, $p_i=y_{0,i}/y_{0,1}$, is introduced. Then Eq. (2) can be written as:

$$\frac{dy_i}{dt} = -\alpha_i y_1 + \beta_i y_f(1-y_i), \quad (3a)$$

$$\frac{dy_f}{dt} = p_i\sum_{i=1}^{N}[\alpha_i y_i - \beta_i y_f(1-y_i)] - \gamma y_f\left(\sum_{i=1}^{N} p_i y_i + y_f\right). \quad (3b)$$

Eq. (3) can be solved by using the numerical method of Runge–Kutta [12]; the parameter values are at first found by trial and error and later refined by the grid optimization method [28].

At the beginning we consider the case of a single structural configuration of hole traps and the parameter values thus determined are shown in Table 1. Unfortunately, these values do not obey a regular $\sqrt{T}$ temperature dependence, expected from the results of data analysis and theoretical modeling [21–24], and hence we should discard this case.

Next we examine the case of two different structural configurations of hole traps. Table 2 indicates the parameter values obtained. It is noted from the table that two parameters β_2 and γ change with temperature according to the regular temperature dependence mentioned above, whereas the parameter β_1 decreases with increasing the temperature, contrary to the regular temperature dependence. Consequently, we discard this case.

We finally consider the model of O^- bound small polarons, proposed by Schirmer and Krambrock, in which the O^- polarons adjacent to single kind recombination centers are assumed to have two different structural configurations. A theoretical study on intrinsic defects in topaz indicates the favored formation of fluorine ion F^- vacancies [29]. These vacancies require charge compensation and Cl^- ions, for example, serve as a charge compensator. Under gamma irradiation, the O^- hole center is created, as mentioned before, at the OH^- lattice site removing the hydrogen from the OH^- ion. We presume that gamma irradiation replaces the charge compensators by electrons released in this process and that, during heating, the holes in the O^- hole centers are thermally released and recombined with the electrons trapped in the F^- vacancies. The F^- and OH^- sites in the octahedral structure are adjacent [30] and hence this recombination should be first-order kinetics. It is found through trial and error that, if $\beta_i/\gamma \geq 600$, the solutions of kinetic equations become insensitive to changes in β_i and can be approximately given by a sum of exponential decays of first-order kinetics.

Using the grid optimization method [18,31] we can determine the parameters α_1, α_2 and $p=y_{0,2}/y_{0,1}$ for the two different configurations of O^- polarons. The deviations from the respective best-fit parameter values thus determined, due to the fitting procedures and inaccuracy in determination of the optical absorption band intensities, are calculated. Concerning the former deviations, we calculate the cost functions increasing or decreasing the parameter values from the respective best-fit parameter values and adopt, as the deviation from each best-fit parameter value, the largest difference in magnitude between the best-fit parameter value and a parameter value giving a 20% increase in cost function [32]. Table 3 presents the best fitted parameters with the respective deviations obtained for the isothermal decay analysis and each solid line shown in Fig. 3 is the best fit; the average of the values given in Table 3 for the parameter p is 1.69 ± 0.23. It is important to note here that the process involving the retrapping of free holes is negligible. The activation energies determined are $E_1=0.88\pm0.13$ eV for α_1 and $E_2=0.52\pm0.08$ eV for α_2.

5. Simulation of 400 nm monochromatic TL glow curve data

We have determined in Section 4 the kinetic parameters from the isothermal decay analysis for the 620 nm absorption band, on the basis of O^- bound small polarons in two structural configurations. From the facts that: the 620 nm absorption band in blue topaz is attributed to the O^- bound small polarons; this absorption band can be further associated with the TL emission at 400 nm, as mentioned in Section 3.1, a convenient way to describe this TL emission can be as follows. Heating imparts activation energy to the O^- hole centers from which the holes become released and immediately migrate to adjacent single type electron traps (electrons trapped in F^- vacancies). Recombination of these holes with the electron traps (recombination centers) results in energy that is spent in inducing luminescence. Thus, the TL peak temperature is determined by the activation energy, and the TL spectrum is determined by the characteristics of the recombination center. In this section we attempt to simulate a monochromatic TL glow curve at 400 nm, using the kinetic parameters determined.

Table 1
Fit parameters in case of a single structural configuration of the hole traps for the isothermal decay of 620 nm absorption band.

T(K)	α (10^{-7} s)	β (10^{-5} s)	γ (10^{-6} s)
515	4.52 ± 0.16	9.4 ± 8.9	46.3 ± 5.2
523	8.89 ± 0.61	0.068 ± 0.010	0.214 ± 0.037
562	90.6 ± 5.6	6.50 ± 0.61	6.9 ± 1.7
693	112.4 ± 2.5	1.63 ± 0.28	73 ± 31

Table 3
Fit parameters in case of two different structural configurations of O^- poralons for the isothermal decay of 620 nm absorption band.

T(K)	α_1 (10^{-7} s)	α_2 (10^{-7} s)	p
515	0.147 ± 0.053	6.6 ± 3.1	1.31 ± 0.19
525	0.63 ± 0.18	14.3 ± 1.8	1.95 ± 0.34
562	1.52 ± 0.32	32.2 ± 3.1	1.83 ± 0.28
693	41 ± 12	180 ± 24	1.68 ± 0.78

Table 2
Fit parameters in case of two different structural configurations of the hole traps for the isothermal decay of 620 nm absorption band.

T(K)	α_1 (10^{-7} s)	β_1 (10^{-5} s)	α_2 (10^{-6} s)	β_2 (10^{-6} s)	p	γ (10^{-5} s)
515	0.317 ± 0.056	10.31 ± 0.011	0.613 ± 0.006	3.02 ± 0.54	1.68 ± 0.19	1.00 ± 0.21
523	0.317 ± 0.089	8.806 ± 0.055	1.43 ± 0.03	5.57 ± 0.29	3.00 ± 0.87	1.48 ± 0.18
562	2.06 ± 0.61	4.87 ± 0.16	3.83 ± 0.12	12.6 ± 0.7	2.43 ± 0.54	2.04 ± 0.19
693	606 ± 25	2.04 ± 0.06	8.9 ± 1.1	21.1 ± 7.8	5.1 ± 1.8	15.6 ± 7.2

Experimentally, the monochromatic TL glow curve data at 400 nm can be extracted from the TL emission spectra observed during the heating of the sample shown in Fig. 1. These data extracted are depicted in Fig. 5 as a function of heating time (dots); the error bars in the figure were estimated from the variation in time during the measurement of each TL emission spectrum and inaccuracy in determination of the TL emission intensity at 400 nm. Assuming that a heating manner in an interval of time between one point (t_{j-1}) and the following point (t_j) in Fig. 1 is linear, a TL glow curve can be given by a sum of TL intensities over M intervals of time [33–36]. The mathematical expression of the TL glow curve for a single activation energy and first-order kinetics, $I(t)$, is given by:

$$I(T) = n_0 s_i \sum_{j=1}^{M} \exp(-E_i/kT_j)\exp\{-s\int_{t_{j-1}}^{t_j} \exp[-E_i/kT(t)]dt\}, \quad (4)$$

where n_0 is the initial concentration of hole traps and T_j is the absolute temperature at the end of the j-th interval of time.

In this study there are two activation energies obtained, $E_1 = 0.88 \pm 0.13$ eV and $E_2 = 0.52 \pm 0.08$ eV. The thermal release processes regarding the two activation energies may be independent and hence the monochromatic TL glow curve at 400 nm is given by a sum of the TL intensity due to E_1 and that due to E_2. The ratio of the TL intensity due to E_2 relative to that due to E_1 is equal to p, that is, the ratio of the initial concentration of the hole traps related to E_2 relative to that to E_1. The simulation results using the two activation energies and $p = 1.68 \pm 0.40$ is indicated in Fig. 5 (solid line).

From the figure the simulation result can be considered to be in accord with the experimental result; two unambiguous peaks are observed in both the experimental and simulation results. As mentioned previously, this finding reflects the two different activation energies of O^- hole traps, responsible for the 620 nm absorption band, and the presumption of single type electron traps indicates a single TL emission spectrum. Hence, it is concluded that thermal annealing of this absorption band causes the 400 nm TL emission band.

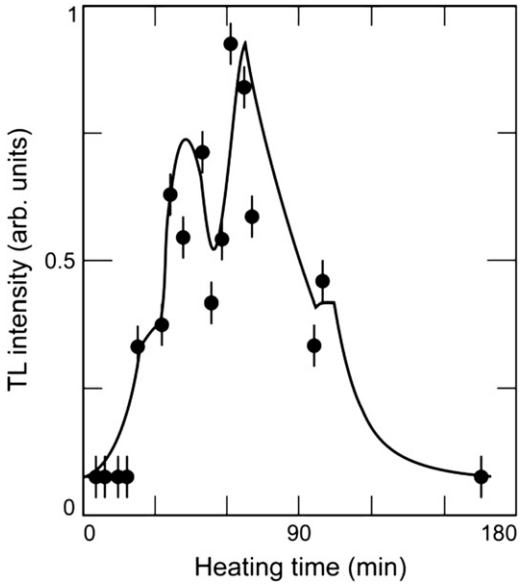

Fig. 5. Normalized monochromatic TL glow curve at 400 nm, extracted from the TL emission spectra measured, as a function of heating time (dots). The solid line shows the simulation result.

6. Conclusion

In this study the TL emission spectra observed in blue topaz are found to have two bands at 400 and 800 nm; the first is observed alone in 373–553 K and the second appears above 553 K. The thermal decay of the 620 nm absorption band takes place in the temperature region of 373–553 K in which the 400 nm TL emission band is present. Hence, the isothermal decays for the 620 nm absorption band are measured at 515, 523, 562, and 693 K with the intention of determining their kinetic parameters and correlating subsequently this absorption band with the 400 nm TL emission band.

On the other hand, Krambock et al. [9] suggest that the 620 nm absorption band may originate from the O^- hole centers. Accordingly, these isothermal decay curves are analyzed by using the two differential equations describing the kinetics of N different structural configurations of O^- hole centers and a single type of recombination centers. On the basis of the model proposed by Krambock et al. [9], in which O^- bound small polarons are adjacent to trapped electrons (electrons in the F^- vacancies are presumed in this study), two different configurations of O^- polarons and first-order kinetics are found to explain nicely the isothermal decay curves; two activation energies, 0.52 ± 0.08 and 0.88 ± 0.13 eV, and the parameter $p = 1.69 \pm 0.23$, defined as the ratio between the initial concentrations of two different configurations of O^- polarons, are determined. This knowledge can explain reasonably the monochromatic TL glow curve data at 400 nm extracted from the TL emission spectra observed, indicating two different structural configurations of O^- polarons responsible for the 620 nm optical absorption band and the thermal annealing of these defects induces the 400 nm TL emission band.

Acknowledgments

The present work was partly supported by grants from the Conselho Nacional de Desenvolvimento Científico (CNPq), Fundação de Amparo à Pesquisa de São Paulo (FAPESP), Secretaria de Ciência e Tecnologia (RHAE) and Financiadora de Estudos e Projetos (FINEP).

References

[1] W.A. Deer, R.A. Howie, I. Zussman, An Introduction to the Rock-Forming Minerals, 2, Longman, London, 1978.
[2] S.C. Lind, L. Bardwell, Am. Mineral. 8 (1923) 171.
[3] K. Nassau, B.E. Prescott, Am. Mineral. 60 (1975) 705.
[4] V. Priest, D.L. Cowan, D.G. Reichel, F.K. Ross, J. Appl. Phys. 68 (1990) 3035.
[5] D.N. da Silva, K.J. Guedes, M.V.B. Pinheiro, S. Schweizer, J.-M. Spaeth, K. Krambrock, Phys. Status Solidi (c) 2 (2005) 397.
[6] D.N. da Silva, K.J. Guedes, M.V.B. Pinheiro, J.-M. Spaeth, K. Krambrock, Phys. Chem. Miner. 32 (2005) 436.
[7] A.S. Leal, K. Krambrock, L.G.M. Ribeiro, M.A.B.C. Menezes, P. Vermaercke, L. Sneyers, Nucl. Instrum. Methods Phys. Res. A 580 (2007) 423.
[8] O.F. Schirmer, J. Phys. Condens. Matter 18 (2006) R667.
[9] K. Krambrock, L.G.M. Ribeiro, M.V.B. Pinheiro, A.S. Leal, M.A.B.C. Menezes, J.-M. Spaeth, Phys. Chem. Miner. 34 (2007) 437.
[10] A.R.P.L. Albuquerque, Sadao Isotani, S.P. Morato, Radiat. Eff. Defects Solids 106 (1988) 143.
[11] E.I. Adirovitch, J. Phys. (France) 17 (1956) 705.
[12] P. Kelly, M.J. Laubitz, P. Braunlich, Phys. Rev. B 4 (1971) 1960.
[13] O.L. Dias, A.R.P.L. Albuquerque, S. Isotani, An. Acad. Bras. Cien. 55 (1983) 173.
[14] W. Bonventi Jr., S. Isotani, A.R.P.L. Albuquerque, Adv. Condens. Matter Phys. 2012 (2012) 1.
[15] G. Lehmann, H. Harder, Am. Mineral. 55 (1970) 98.
[16] D.S. Goldman, G.R. Rossman, Am. Mineral. 67 (1982) 340.
[17] M.N. Taran, M. Koch-Muller, Phys. Chem. Miner. 33 (8) (2006) 511.
[18] C.T. Dotto, S. Isotani, Radiat. Eff. Defects Solids 117 (1991) 355.
[19] M.V.B. Pinheiro, C. Fantini, K. Krambrock, A.I.C. Persiano, M.S.S. Dantas, M.A. Pimenta, Phys. Rev. B65 (2002) 104301.
[20] J.T. Kloprogge, R.L. Frost, Spectrochim. Acta Part A 56 (2000) 501.
[21] S. Isotani, W.W. Furtado, R. Antonini, O.L. Dias, Am. Mineral. 74 (1989) 432.

[22] R. Antonini, S. Isotani, W.W. Furtado, W.M. Pontuschka, S.R. Rabbani, An. Acad. Bras. Cien. 62 (1990) 39.
[23] S. Isotani, A.T. Fujii, R. Antonini, W.M. Pontuschka, S.R. Rabbani, W.W. Furtado, An. Acad. Bras. Cien. 62 (1990) 107.
[24] S. Isotani, W.W. Furtado, R. Antonini, A.R. Black, W.M. Pontuschka, T. Tomé, S.R. Rabbani, Phys. Rev. B42 (1990) 5966.
[25] P. Durand, Y. Farge, M. Lambert, J. Phys. Chem. Solids 30 (6) (1969) 1353.
[26] Y. Farge, J. Phys. Chem. Solids 30 (6) (1969) 1375.
[27] W.W. Furtado, T. Tome, S. Isotani, R. Antonini, A.R. Black, W.M. Pontuschka, S.R. Rabbani, An. Acad. Bras. Cien. 61 (1989) 397.
[28] S. Isotani, A.T. Fujii, Comput. Phys. Commun. 151 (2003) 1.
[29] R.A. Jackson, M.E.G. Valerio, J. Phys. Condens. Matter 16 (2004) S2771.
[30] D.N. da Silva, K.J. Guedes, M.V.B. Pinheiro, J.M. Spaeth, K. Krambrock, Phys. Chem. Miner. 32 (2005) 436.
[31] S. Isotani, K. Watari, A. Mizukami, W. Bonventi Jr., A.S. Ito, Physica B 391 (2007) 322.
[32] S. Isotani, A.R. Blak, S. Watanabe, Physica B 405 (2010) 1501.
[33] J.T. Randall, M.H.F. Wilkins, Proc. R. Soc. London 184 (1945) 365.
[34] M.S. Raseed, J. Fluoresc. 15 (4) (2005) 485.
[35] R. Chen, Y. Kirsh, Analysis of Thermally Stimulate Processes, Pergamon, Oxford, 1981, p. 167.
[36] R. Chen, S.W.S. McKeever, Theory of Thermoluminescence and Related Phenomena, World Scientific, Singapore, 1997, p. 262.